PAPER • OPEN ACCESS

Frequency scanning interferometry based deformation monitoring system for the alignment of the FCC-ee machine detector interface

To cite this article: Léonard Watrelot *et al* 2023 *Meas. Sci. Technol.* **34** 075006

View the article online for updates and enhancements.

You may also like

- Frequency scanning interferometry in ATLAS: remote, multiple, simultaneous and precise distance measurements in a hostile environment
  P A Coe, D F Howell and R B Nickerson

- Spectroscopically *in situ* traceable heterodyne frequency-scanning interferometry for distances up to 50 m
  Günther Prellinger, Karl Meiners-Hagen and Florian Pollinger

- Absolute distance measurement using frequency sweeping interferometry with large swept range and target drift compensation
  Shihua Zhang, Hao Jin, Lingqi Zhang et al.

Frequency scanning interferometry based deformation monitoring system for the alignment of the FCC-ee machine detector interface

Léonard Watrelot[1,2,*] ⓘ**, Mateusz Sosin**[1] ⓘ **and Stéphane Durand**[2] ⓘ

[1] CERN,1 Esplanade des Particules, Meyrin 1211, Genève, Switzerland
[2] Cnam/GeF, 1 Boulevard Pythagore, Le Mans 72000, France

E-mail: leonard.watrelot@cern.ch

CrossMark

Abstract

In a particle accelerator, two particle beams are accelerated and collided at one or several physics detectors. The machine detector interface (MDI) is the place where the accelerator ring is linked to the physics detector. It is the area where the alignment requirements are the most stringent, and the MDI of the lepton version of the future circular collider (FCC-ee) is no exception. It will implement a complex design and alignment requirement for typical components in the MDI are of the order of 30 μm. Until now, no working solutions have been proposed for the alignment of such MDI. In this contribution, two different systems are studied: the Surveillance d'Ouvrages par Fibre Optique (Structural Monitoring by Optical Fibers, SOFO) and the in-lined multiplexed and distributed frequency scanning interferometry (FSI). Both systems allow individual and simultaneous distance measurements of multiple portions along a fiber, and a new system using the FSI technology is proposed for the alignment monitoring. Using a network of helical shaped fiber allows the measurement of deformations if a sufficient amount of fibers is placed on the cylinder. With a sensor measurement accuracy of 1 μm, 3D coordinates of points at the end of a 4 m long and 0.25 m radius cylinder (FCC-ee MDI dimensions) can be determined at an accuracy under 5 μm. This system will provide a link between the alignment of the final focusing quadrupoles and the rest of the machine.

(Some figures may appear in colour only in the online journal)

1. Introduction

The future circular collider (FCC) aims to be the next flagship project in 35 years at CERN after the High Luminosity upgrade of the Large Hadron Collider (LHC). A 93 km long circular tunnel will host the two planned stages of the machine, a lepton version (FCC-ee) and a hadron version (FCC-hh) [1]. For the FCC-ee, the tunnel will host four caverns for the physics experiments. The machine detector interface (MDI) is the area where the colliding beams circulating in the accelerator are finely focused to reach 6.4×0.028 μm size against $>500 \times 500$ μm in the rest of the machine [2]. The smallest sized beams of the entire ring, need to be very precisely steered from two ends of the accelerator separated by a detector, to

---

* Author to whom any correspondence should be addressed.

collide as precisely as possible in the center of the physics experiment. Having a better alignment allows for bigger the sections of the beams to intersect at the interaction point (IP) and more collisions per cm^2 per second to be produced, which corresponds to the luminosity of the collider and can be interpreted as its performance. Therefore, the alignment of the elements on the beam line in that region is critical. In the FCC-ee, the last accelerator components are located inside the physics detector, where the conditions are particularly harsh and the space very limited. The alignment and monitoring of these final components inside the detector could facilitate machine operation, improve physic measurements and avoid critical luminosity loss. But such alignment and monitoring has never been implemented so far [3]. Both the space and harsh condition made the optical, capacitive and known interferometric sensors unusable in this configuration. The difficulty of the situation is also underlined by the absence of solutions for projects such as CLIC [4] or ILC [5]. The objective of this research was to design an alignment and monitoring system for the FCC-ee MDI, in order to meet optical requirements in terms of alignment requirements while also meeting mechanical requirements with respect to the lack of space and the harsh conditions. The strategy for the alignment of the FCC-ee MDI will stand on three sub-systems: an external monitoring system, a deformation monitoring system and an internal monitoring system. The internal monitoring system will measure the inner components with respect to the solenoid support with a cylinder shape located inside the detector. The solenoid support is then monitored by the deformation monitoring system, with respect to an interface toward the outside of the detector. This interface will finally be monitored thanks to the external alignment system, allowing the alignment between the inner components and the rest of the machine. This paper will focus on the deformation monitoring system, which is the most complex sub-system, located in harsh conditions and extremely tight space.

2. Deformation model

2.1. FCC-ee MDI design

In order to optimize the luminosity of the machine, and therefore increase the collider's performance, the FCC-ee will implement a crab-waist configuration. This configuration can be obtained by having a big Piwinski angle, which can be done by increasing the crossing angle of the two beams at the IP and by decreasing the horizontal beam size [6]. These specifications imply to have a complex MDI as described in the conceptual design report [2]: an assembly with a 3.6 m long and 0.25 m radius vacuum vessel with a cylindrical shape ended by a truncated cone 0.77 m long and going from 0.25 m radius to 0.1 m radius will be located inside the detector, in a cantilever configuration held from outside the detector. Figure 1 describes this assembly, which is composed of a skeleton, supporting the beam pipe surrounded by the final focusing quadrupoles and the beam position monitors (BPM). This skeleton also holds the support for the screening and compensation solenoids, and two additional solenoids
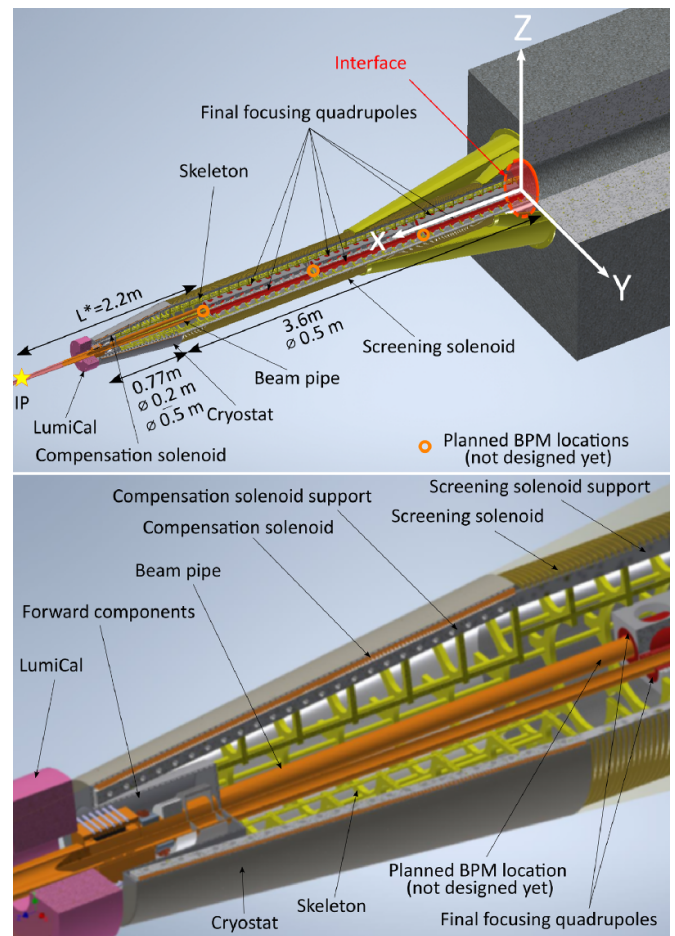
Figure 1. Inner components, original assembly. On the top picture, a general view of the assembly and the coordinate system associated to the plate. The second picture is zoomed in order to see the different elements, from the inside out: the beam pipe (orange), the final focusing quadrupoles (red), the skeleton (yellow), the support and cooling structure for the solenoids (gray), the screening and compensation solenoids (orange) and the thin cryostat (gray). The free length (L*) corresponds to the distance between the IP and the face of the closest quadrupole. The interface used as reference for the deformation monitoring system is placed at the outer end of the assembly.

whose purpose is to protect the final focusing quadrupoles and the beam from the experiment magnetic field. The entire assembly is covered by a thin vacuum vessel cryostat as the interior will be cooled down to cryogenic temperatures for the solenoids and final focusing quadrupoles to reach superconducting state. The goal of the alignment monitoring system is to study the alignment of most of the inner components (final focusing quadrupoles, BPM, solenoids) and the luminosity calorimeters (LumiCal) located at the far end toward the IP.

To achieve that objective, first the assembly deformation will be monitored. The studied parts for the deformation are the solenoid supports, which have simple geometric shapes (a cylinder and a truncated cone) in direct contact with the skeleton. This will supply a precise set of points that can be used as s reference for the inner alignment monitoring, measuring the final focusing quadrupoles and BPM.

Deformations will be studied with respect to a circular plate placed at the end of the assembly, towards the outside sides of the detector. This plate will serve as an interface to link the inner alignment and the outer one, to check the alignment of the inner components with respect to the rest of the machine, and the alignment of both sides of the experiment. This interface is placed at the most stable place of the assembly, close to the support of the assembly towards the outside of the detector as it can be seen on figure 1.

2.2. Creation of a deformation model

Deformations are defined in the (O, O_x, O_y, O_z) Euclidean system linked to the interface plate, shown in figure 1. The origin of this system is the center of the plate, the O_x is perpendicular to the plate, O_y is the intersection of the plane of the plate and the plane formed by the incoming and outgoing beams, crossing at a 30 mrad angle at the IP [2]. O_z is the last vector in order to form an oriented orthogonal system. It is important to note that this O_z vector is not along the beam direction like for the physicist definition, but towards the zenith like the surveyors' definition. In that system, as shown in (1), we can express the usual (x, y, z) point coordinates thanks to a set of functions to later include deformations and to compute point positioning formal precision:

$$\begin{cases} C_X(x,y,z) = x \\ C_Y(x,y,z) = r\sin(\phi), \quad \text{with} \quad \phi = \arctan 2(y,z) \\ C_Z(x,y,z) = r\cos(\phi) \end{cases} \quad (1)$$

Parameters of the point definition are represented on figure 5. It is interesting to note that, without any deformation: $C_X(x,y,z) = x$, $C_Y(x,y,z) = y$, $C_Z(x,y,z) = z$.

As the design is still at an early stage and not mature enough to do precise deformations computations with computer assisted design software, the deformations have been simulated thanks to a Python software developed for the study. The deformations were generated thanks to the six deformation polynomials are used, as indicated in (2) allowing to simulate a wide range of deformations.

$$\forall u \in \mathbb{R}$$

$$P_x(u) = \sum_{i=0}^{n} a_i u^i, \ P_y(u) = \sum_{i=0}^{n} b_i u^i, \ P_z(u) = \sum_{i=0}^{n} c_i u^i,$$

$$P_\theta(u) = \sum_{i=0}^{n} d_i u^i, \ P_{ry}(u) = \sum_{i=0}^{n} e_i u^i, \ P_{rz}(u) = \sum_{i=0}^{n} f_i u^i \quad (2)$$

With $n \in \mathbb{N}$ and $\forall i \in [\![0;n]\!]$, $a_i, b_i, c_i, d_i, e_i, f_i \in \mathbb{R}$.

Visualization of the impacts of these polynomials were generated in python and shown in figure 2. Each of the polynomials has been applied one by one to a cylinder with the same characteristics as the screening solenoid support, and in the Cartesian coordinate system of the interface: the first deformation is the longitudinal deformation P_x. The two following deformations modeled by P_y and P_z are radial deformations. Then there is a torsion P_θ and finally two radius deformations
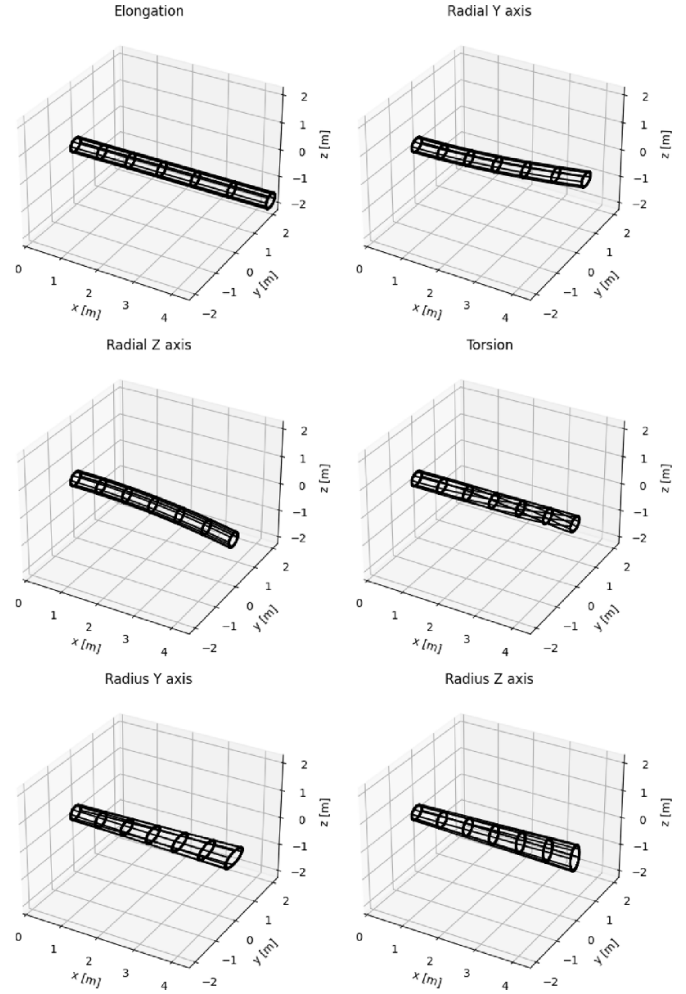
Figure 2. Deformation model visualization (magnified approximately 1000 times) from top to bottom and left to right: longitudinal deformation, radial deformation in the horizontal plane, in the vertical plane, torsion and finally radius deformation in the horizontal plane and in the vertical plane.

P_{ry} and P_{rz} which model the flattening of the cylinder in both directions. Thanks to these polynomials, we are able to model the deformed cylinder, subject to all the forces endured by the assembly once in the detector (gravity, Lorentz force, cooling effects, and so on). It is important to note that the constant values correspond to assembly and initial installation, and therefore will be determined and monitored by an initial calibration and the external monitoring system.

In case of deformations, the coordinates of the points stated in (1) are expressed as:

$$\begin{cases} C_{Xd}(x,y,z) = x + P_x(x) \\ C_{Yd}(x,y,z) = (r + P_{ry}(x))\sin(\phi + P_\theta(x)) + P_y(x) \\ C_{Zd}(x,y,z) = (r + P_{rz}(x))\cos(\phi + P_\theta(x)) + P_z(x) \end{cases} \quad (3)$$

2.3. Simulations

As the design is still at an early stage and mechanical simulation on the structure have not started yet, the deformation
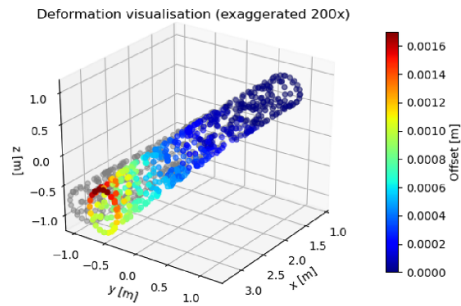
Figure 3. Comparison of a set of points (gray) and the set of deformed points colored as a function of the distance between the original and deformed point.

simulations were made to represent the largest possible range. The only known limit so far is the 2 mm maximum deformation allowed for the assembly to avoid any physical contact with the detector. A coefficient generator was used to create coefficients sets, which were then filtered to keep only the realistic ones. A realistic coefficient set is defined as a set which, once applied to any point on the cylinder, does not create an offset bigger than 2 mm between the original point and the deformed point (to ensure that the mechanical limitation is respected). Figure 3 shows offsets computed for one coefficient set. The representation is voluntarily magnified 200 times in order to visualize the deformation.

3. New sensor technology

3.1. Limits of current sensors

The area where the alignment monitoring system needs to be installed is very complex and conditions are harsh. Current sensors are not suitable for this area. Optical sensors such as Brandeis CCD Angle Monitors (BCAM) which are used in ATLAS could not withstand the radiations [7] while wire positioning systems and hydrostatic leveling systems used in the LHC MDI for example, require additional infrastructure to work (stable support pillars, water network, stable wire anchoring points, clear line of sight …) which cannot be provided. Classical frequency scanning interferometry (FSI) distance measurement sensors have no direct implementation possible in the MDI and other types of sensors are facing similar problems, as underlined by the absence of solution for other projects (CLIC, ILC). An interesting solution comes from fiber deformation measurements, nowadays mostly used in civil engineering [8, 9] or aerospace industry [10]. These sensors have multiple advantages, as they are really precise and accurate while being resistant to all the conditions that can be found in the assembly and not taking too much space. Moreover, they are passive sensors, implying no perturbations around the measurement area. Currently, they can measure 1D [8, 9] or 1D+1D deformations [8]. Two different systems could be used for this deformation monitoring and are studied in this contribution: the Surveillance d'Ouvrages par Fibre Optique (Structural Monitoring by Optical Fibers, SOFO) system and the FSI technology.

3.2. SOFO

The SOFO system is an extremely precise fiber optic displacement sensor with long term stability, currently commercialized by SMARTEC in Switzerland [9]. It is composed of two parts: a sensor and a separated reading unit. The measurement principle is based on a low coherence double Michelson interferometer. The first interferometer is composed of the measurement fiber, which is mechanically coupled to the monitored structure and follows its deformations, while the other arm is a reference fiber installed freely inside a pipe and acting as a temperature reference. The analysis is done thanks to the second Michelson interferometer with one of the arms terminated with a mobile mirror introducing an accurately known path difference between the two arms.

This simple fiber length measurement allows an operation in harsh conditions without affecting the surroundings. By using partial reflectivity mirrors along the fiber, one fiber can also have multiple and independent measuring portions (up to ten) with an RMS accuracy always lower or equal to 3 µm [11].

3.3. FSI

The frequency scanning interferometry (FSI) system is very similar to a Michelson interferometer, from which the constant frequency laser is replaced by a scanning laser source [12]. This laser goes through a fiber with a ferrule tip used as a reference mirror, reflecting around 4% of the light, forming the reference arm of the interferometer. The transmitted light goes towards a reflective target to determine the distance from the ferrule to the target. The classical FSI, based on fringes counting, allows only to measure single distances, and it is sensitive to power of reflected light. The second approach, currently used at CERN bases on Fourier analysis of interference beat frequencies [12]. It allows for multiple targets measurements, and it is less sensitive to reflected light power variations Currently, this technology is used to measure distances in air and vacuum, to corner cube retro-reflectors, glass bead and a water surface [13–17]. Nevertheless, it can be easily extended to measurements in the fibers. Such an 'in-fiber' measurement is currently developed at CERN called the in-lined multiplexed and distributed FSI. This type of measurement is carried out by putting two consecutive semi-reflective mirrors in the fiber (the two ends of interferometer arms), allowing the monitoring of the 3D length of the fiber between these two mirrors. This technology also allows more than two semi-reflective mirrors in order to do multiple and independent measuring portions along the fiber.

4. Deformation monitoring system

4.1. Layout

With these new in-fiber length monitoring sensors, it is possible to monitor the cylinder shape in 3D, by gluing the fiber in a helix shape inside the supports of the solenoids as shown in the top picture of figure 4. This gluing can be very similar
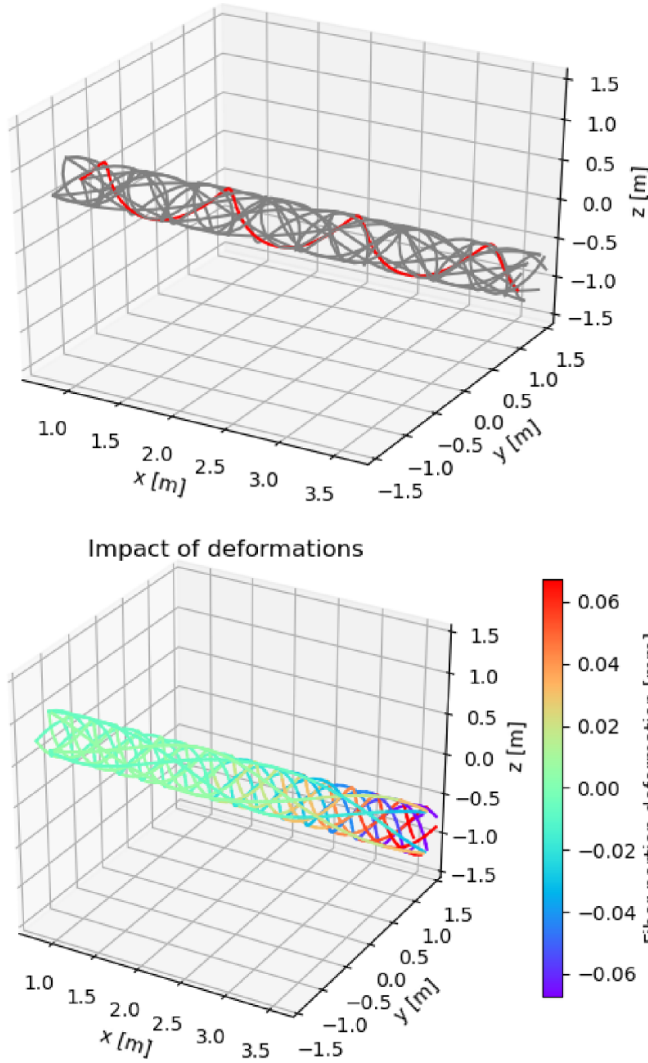
Figure 4. Examples of a network of fibers: the top picture represents a fiber network with a helical shape along the cylinder, with one individual fiber highlighted; the bottom picture represents an example of the deformation impact over that network. The colors represent the elongations or contractions values of the portion of the fiber.

to the precise winding of magnets. The physical dependence created will allow the fiber to monitor the shape of the cylinder. By knowing the impact of the deformation on the portion lengths and by monitoring these lengths, it is possible to compute the deformation thanks to the least squares adjustment process. This has several advantages, as helices are able to monitor all the deformations at once (as opposite to straight longitudinal fibers, for example). This allows a good redundancy in the fiber network in case of any mis-installation or damage to a fiber. Moreover, deformations on the cylinder will have a smaller impact on the fiber deformation compared to longitudinally placed fibers, for example, which may help to avoid any breaking.

4.2. Computation

Once placed according to helices shape on the cylinder, the fibers follow a 3D curve described by the formulas in
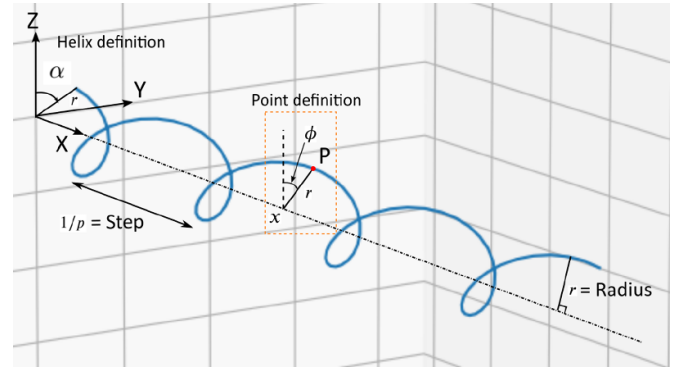
Figure 5. Drawing of a helix and a point, with the parameters defining them.

equation (3), with respect to the reference system (O, O_x, O_y, O_z) previously defined:

$$\begin{cases} h_x(x) = x \\ h_y(x) = \varepsilon r \sin\left(\dfrac{x}{p} + \alpha\right) \\ h_z(x) = r \cos\left(\dfrac{x}{p} + \alpha\right) \end{cases} \tag{4}$$

Where ε corresponds to ± 1 to define if the helix is right-handed or left-handed, r corresponds to the radius of the helix, $1/p$ corresponds to the step and α corresponds to the angle in the (O, O_y, O_z) plane from which the helix starts. These parameters are represented on figure 5. The impact of deformations on these helices can be modeled by adding the polynomials to (4) resulting in (5):

$$\begin{cases} h_{xd}(x) = x + P_x(x) \\ h_{yd}(x) = \varepsilon \left(r + P_{ry}(x)\right) \sin\left(\dfrac{x}{p} + \alpha + \varepsilon P_\theta(x)\right) + P_y(x) \\ h_{zd}(x) = \left(r + P_{rz}(x)\right) \cos\left(\dfrac{x}{p} + \alpha + \varepsilon P_\theta(x)\right) + P_z(x) \end{cases} \tag{5}$$

Figure 6 shows the portion p_u between two consecutive semi-reflective interfaces located at the abscissas x_{u1} and x_{u2}, which distance is expressed in (6):

$$d(p_u) = \int_{x_{u1}}^{x_{u2}} \sqrt{\dot{h_{xd}}(x)^2 + \dot{h_{yd}}(x)^2 + \dot{h_{zd}}(x)^2} \, \mathrm{d}x. \tag{6}$$

In this equation $\dot{h}(x)$ corresponds to the derivative of the function $h(x)$ with respect to the variable x.

This equation links the portion length of a helix portion with deformation coefficients. With enough helices and portions along the cylinder, it is possible to estimate, in the least squares process, the deformation coefficients.

4.3. Output

Although we can obtain the deformation coefficients and their corresponding accuracy, they are not easy to understand and
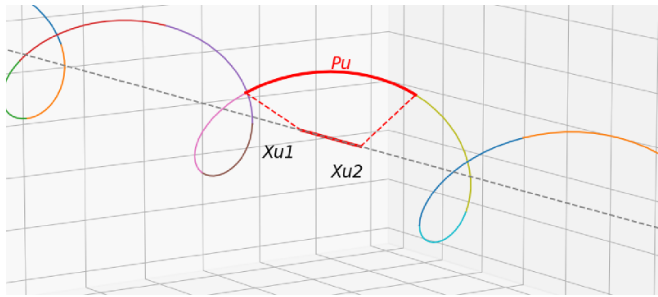
Figure 6. Visualization of a fiber portion p_u between two consecutive semi-reflective interfaces in the fiber located at abscissas x_{u1} and x_{u2}.

to work with. In order to have a data that could be shared more easily, a set of points have been computed and thanks to their expression (taking into account the deformations), it is possible to express the positioning standard deviation thanks to a variance propagation. By deriving (3) with respect to the deformation coefficients and by using the covariance matrix obtained by the least squares adjustment, we can access the point position standard deviation.

5. Simulation and first results

5.1. In-lined multiplexed and distributed FSI system

The very first tests have been conducted on the new FSI system, using a bench to study the feasibility and the initial behavior of the sensor. These tests have been performed in our metrology lab, with temperature and humidity controlled. Figure 7 shows the bench configuration: a reference bar and 3 manually movable parts with micrometric repeatability. Each of this movable parts has a corner cube reflector mounted on it. The tested fiber has three measuring portions and is fixed on the reference bar and all the movable parts as explained on figure 8. The goal was to study the correct functioning of the technology, to estimate the accuracy of each measuring portion, and then to study the eventual impact of deformations of one portion on the others. The measurement campaign, as described in figure 9, was aiming to study each portion independently first and then to deform multiple portions at the same time to study possible impacts of one on another. It also allowed initial accuracy and repeatability tests estimations.

This first measurement campaign, shown on figure 10, confirmed that the system works as expected and that one portion deformation has no impact on the others. Some unknowns still persist regarding the noise and the scale factor that can be seen on the medium and long portion measurements, on the biggest elongations. A big offset could be seen on the small portion measurement at the end of the campaign, where the distance between the movable part and the reference was decreasing to a point where the fiber was sagging, so the 'in-fiber' distance measured did not decrease while the in-air FSI distance did. A glass bead had been placed at the end of the measuring fiber, to see if it could additionally be used as an in-air FSI while monitoring the portion lengths. Results shown on the last picture of
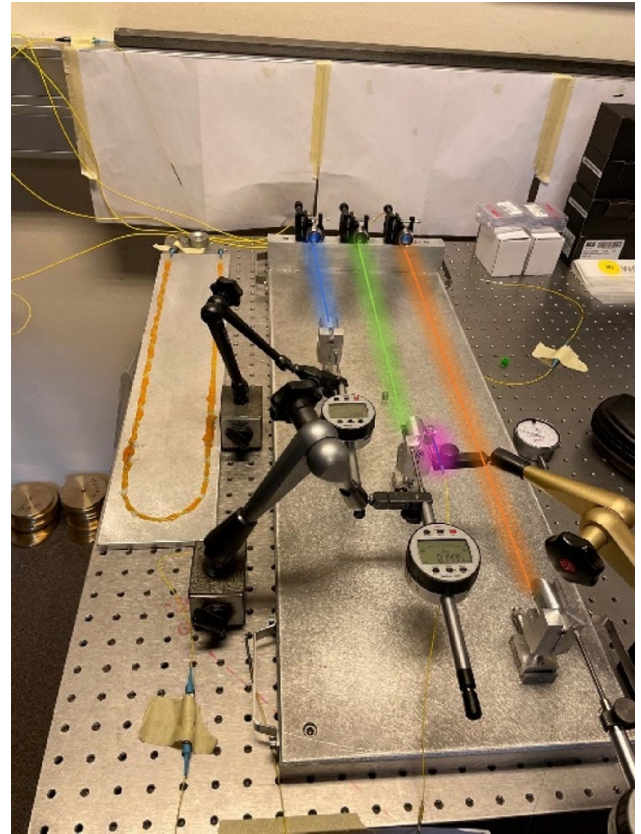

Figure 7. Experimental setup for the FSI 'in-fiber' measurement. The three colored lines are the fiber portions studied, monitored by regular FSI installed in parallel of each portion, measuring on corner cube reflectors. The end of the fiber is also used as a regular FSI, measuring on a glass bead.
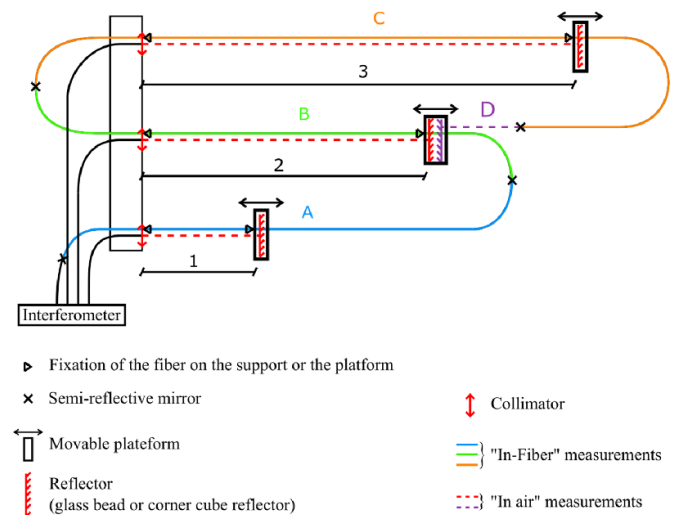
Figure 8. The FSI 'in-fiber' testing bench. Studied stretched fiber portions (A), (B), (C) can have their length changed thanks to the movable platforms and monitored by regular FSI.

figure 10 that this regular use works perfectly even with measuring portions.

Regarding the accuracy of the measurement, an unknown scale factor limits the absolute accuracy of the system to
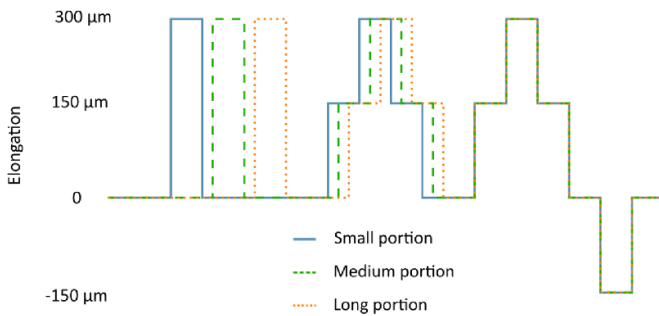
Figure 9. Elongation applied to fiber portions thanks to micrometric movable parts: first, each one of the portions is deformed independently, then they are gradually deformed together, and finally they are all deformed at the same time.

around 30 μm at maximum elongation, while the repeatability is of the order of 10 μm. The main hypothesis for the scale factor that can be seen on the pictures, is the interferometer, which is designed to measure through air and not through glass. This test acts as a proof of concept, showing that it is possible to measure simultaneously and independently multiple portions of a unique fiber. Even though the absolute accuracy is not good enough to be used as it is in the FCC-ee MDI, this was the very first tests and a lot of simple improvements are ready to be implemented in order to make it more accurate, and therefore suitable, for the alignment and monitoring system. Studies on temperature and humidity impact, and the comparison with the in-air FSI, are planned in the near future. This proof of concept encouraged the launch of simulations for the helix shaped network of fibers, aiming to monitor the deformation of the FCC-ee MDI.

5.2. Deformation monitoring system

As the system was still under study, we started by simulating the lengths of the portions of the fibers. We chose a set of realistic deformation coefficients (as described earlier) which were applied to the helices and allowed the computation of the portion lengths as if it was a real network. A random error following a centered normal distribution, with a standard deviation equal to the precision of the measurement 1 μm, have been added to these theoretical length values. The 1 μm value comes from the accuracy of the in-air version of the system, as the fibers were not available at the time the simulations were performed. This is value is also close to the precision of other systems, such as the SOFO system [11].

Knowing the network, using generated observations, the least squares adjustment was performed, and then the point standard deviation was computed, using the variance propagation formula.

The first simulation was conducted by taking a set of deformation smaller than 2 mm, monitored by a network of 36 helices with 100 portion (3600 measurements in total) and an accuracy of 1 μm. Results are summarized in table 1 and figure 12, where the positioning accuracy of 12 points have been highlighted. The 12 points location can be seen of figure 11. Four points are located near the interface, four
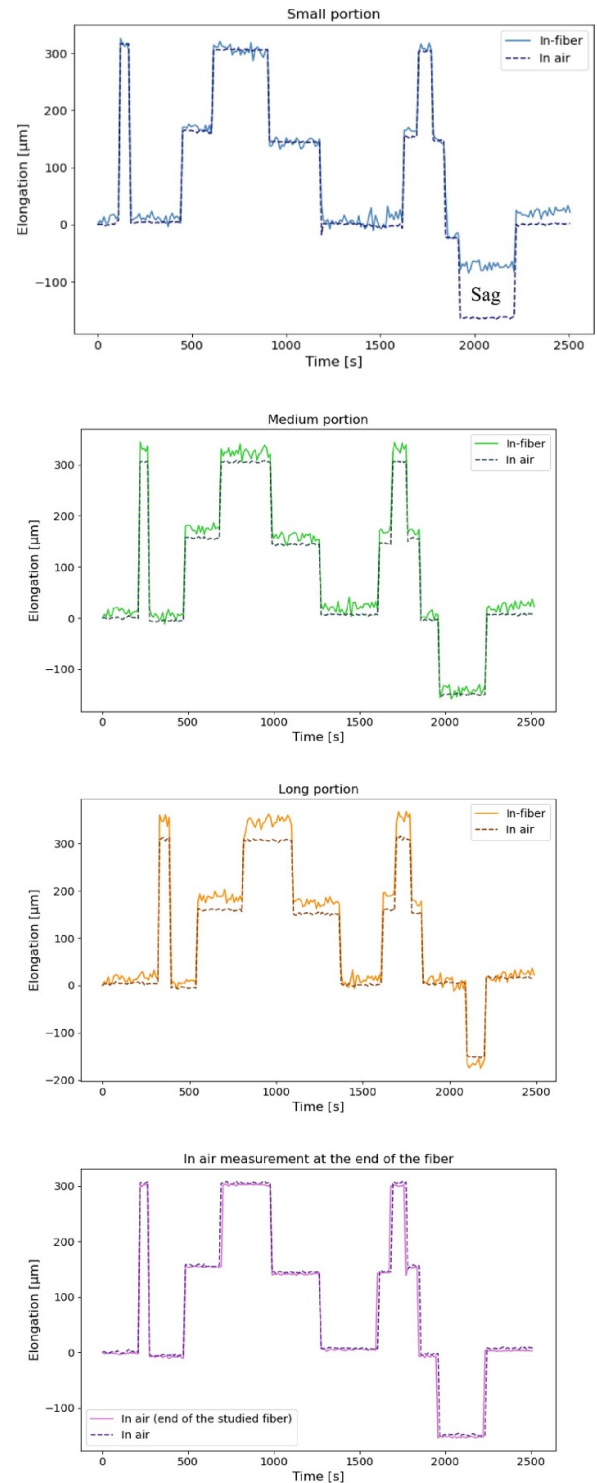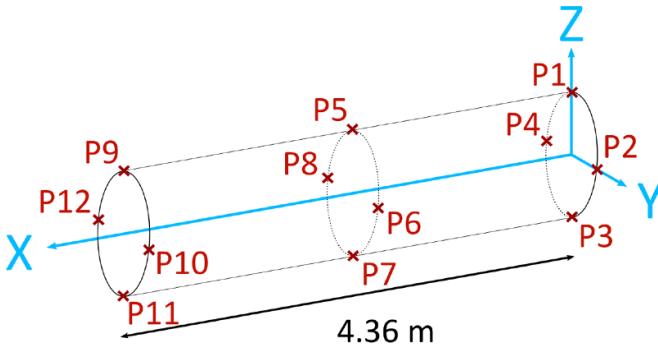

Figure 10. First results of the FSI 'in-fiber' measurements. Each portion has been tested, from top to bottom: small portion, medium portion, long portion and in air measurement done with the end of the studied fiber. The smallest portion studied was subject to sag when decreasing the distance between the platform and the reference, resulting in a decrease of the distance in air but not of the distance measured in fiber.

are in the middle of the cylinder and four are at the end of it. They are placed at each cardinal points in the cylinder sections. Figure 12 shows the positioning accuracy along each

Table 1. Standard deviation for the coordinates of the 12 selected points in micrometers.

Points	Accuracy (μm)		
	X	Y	Z
Pt1	<0.01	0.03	0.03
Pt2	<0.01	0.03	0.03
Pt3	<0.01	0.03	0.03
Pt4	<0.01	0.03	0.03
Pt5	0.23	0.36	0.29
Pt6	0.23	0.29	0.36
Pt7	0.23	0.36	0.29
Pt8	0.23	0.29	0.36
Pt9	0.34	0.53	0.45
Pt10	0.34	0.45	0.53
Pt11	0.34	0.53	0.45
Pt12	0.34	0.45	0.54

Figure 12. Point positioning accuracy of the 500 points randomly scattered on the cylinder (sorted by their longitudinal position). X positions of the points P1 to P12 have been highlighted.

Figure 11. Location of 12 points on the cylinder to study the point positioning accuracy.
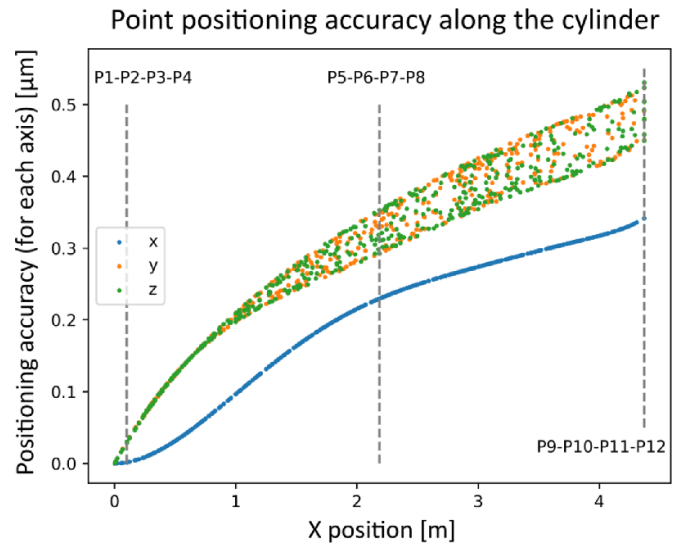
axis of 500 points randomly scattered on the cylinder, sorted by their longitudinal position. The longitudinal positions of the 12 points have been underlined. This picture shows that the accuracy along each axis got worst the further we go from the interface, going from smaller than 0.01 μm to 0.27 μm for the *X* axis and 0.55 μm for the *Y* and *Z* axis.

Even though these are very early stage simulations, the results are promising and modifications to make them more realistic are ongoing. A working direction will be to replace one fiber with a 100 measurement portions by 10 fibers with 10 measurement portions (as it is the current known limit for the SOFO system, for example). Improvement of sensor parts manufacturing and assembly, tests on mis-installation and diverse error identification are also ongoing.

It is also important to note that the deformations simulated on the fiber portions are smaller than 60 μm for a 4 cm long portion, which is well below the fiber stress limit of 1% of the fiber length [18].

5.3. Discussion

Even though a prototype is planned, the technology is still very young and not available yet. For now, the changing of reflected power in the fiber is done by appropriate tightening of two connectors, which creates a thin air gap and acts as an

intra-fiber mirrors on a refractive index transition in the optical path. Though, this system cannot be used in the MDI for space and fiber structure reasons. The same result can be obtained by a 'bad' welding of the fiber, inserting air bubbles in the fiber, but this technique is very inconsistent. Ultimately, the goal would be to UV print the change of refractive index directly in the fiber, not altering the fiber integrity. However, such technique is not easily accessible yet and R&D is required. Regarding the main expected noise sources in the system, one could be due to the change of refractive index and the other due to the Raman, Brillouin and Rayleigh scatterings, which are expected and may require to be mitigated. Mitigation solutions are also already under study, such as a double wavelength interferometer [19] for example, to deal with the scatterings. For now, the FSI system can measure independently and simultaneously in multiple fiber portions, going one step closer toward a helix network of fibers, as a measurement system for the deformations.

6. Conclusion

This paper reports on an innovative and practical design for a deformation monitoring system in the frame of the alignment of the FCC-ee MDI area. A new implementation of the FSI allows the measurement of the fiber length itself. By using this technology and installing it with helices shapes along the measured cylinder, we can determine its deformations. Simulations were done by modeling deformations with polynomials and were solved by the least square adjustment on the helices network. This network allows us to access the coefficients' accuracy, but also point positioning accuracy (thanks to the variance propagation). With this system, 3D point coordinates can be precisely computed to an accuracy of less than 5 μm which is in accordance with the FCC-ee requirements and very promising overall. Studies on network and computation

optimization, making the simulation even more realistic and completing the sensor behavior understanding are the next steps.

Data availability statement

All data that support the findings of this study are included within the article (and any supplementary files).

Acknowledgments

Conflict of interest

The authors declare that they have no known competing financial interests or personal relationships that could have appeared to influence the work reported in this paper.

ORCID iDs

Léonard Watrelot https://orcid.org/0000-0003-4584-7099
Mateusz Sosin https://orcid.org/0000-0003-2148-377X
Stéphane Durand https://orcid.org/0000-0002-9234-6660

References

[1] Benedikt M *et al* 2019 *Future Circular Collider - European Strategy Update Documents* CERN-ACC-2019-0003 (CERN) (available at: https://cds.cern.ch/record/2653669)

[2] Benedikt M *et al* 2018 FCC-ee: the lepton collider: future circular collider conceptual design report volume 2 *Eur. Phys. J. Spec. Top.* **228** 261–623

[3] Watrelot L, Herty A and Durand S 2022 Challenges for the FCC-EE machine detector interface alignment *16th International Workshop on Accelerator Alignment (IWAA)*

[4] Linssen L, Miyamoto A, Stanitzki M and Weerts H 2012 Physics and detectors at CLIC: CLIC conceptual design report (arXiv:1202.5940)

[5] Adolphsen C *et al* 2013 *The International Linear Collider Technical Design Report* (Geneva: Argonne National Lab. (ANL)) (Argonne, IL: Thomas Jefferson) (Comments: See also www.linearcollider.org/ILC/TDR. The full list of signatories is inside the Report. Available from: https://cds.cern.ch/record/1601969)

[6] Zobov M *et al* 2010 Test of 'crab-waist' collisions at the DA Φ NE Φ factory *Phys. Rev. Lett.* **104** 174801

[7] MacKenzie M 2016 ATLAS NSW alignment system radiation tolerance *Senior Thesis* Brandeis University, USA

[8] Chen Z, Zheng D, Shen J, Qiu J and Liu Y 2019 Research on distributed optical-fiber monitoring of biaxial-bending structural deformations *Measurement* **140** 462–71

[9] Inaudi D 1997 Fiber optic sensor network for the monitoring of civil engineering structures *PhD Thesis* (Verlag nicht ermittelbar)

[10] Klotz T, Pothier R, Walch D and Colombo T 2021 Prediction of the business jet Global 7500 wing deformed shape using fiber Bragg gratings and neural network *Results Eng.* **9** 100190

[11] Pozzi M, Zonta D, Wu H and Inaudi D 2008 Development and laboratory validation of in-line multiplexed low-coherence interferometric sensors *Opt. Fiber Technol.* **14** 281–93

[12] Sosin M, Mainaud-Durand H, Rude V and Rutkowski J 2019 Frequency sweeping interferometry for robust and reliable distance measurements in harsh accelerator environment *Proc. SPIE* **11102** 145–61

[13] Kamugasa W S and Vlachakis V 2014 PACMAN study of FSI and micro-triangulation for the pre-alignment of CLIC *13th Int. Conf. on Accelerator Alignment* (CERN)

[14] Kamugasa S W, Gayde J C and Mainaud Durand H 2016 Frequency scanning interferometry for CLIC component fiducialisation *14th Int. Conf. on Accelerator Alignment* (CERN)

[15] Sosin M, Dijoud T, Mainaud Durand H and Rude V 2016 Position Monitoring System for HL-LHC Crab Cavities *7th Int. Particle Accelerator Conf. (IPAC '16) (Busan, Korea, 8–13 May 2016)* (Geneva: JACOW) pp 2704–6

[16] Sosin M *et al* 2021 Robust optical instrumentation for accelerator alignment using frequency scanning interferometry *Measurement* **2** 3

[17] Durand H M *et al* 2018 Frequency scanning interferometry as new solution for the on-line monitoring inside the cryostat for the HL-LHC project *9th Int. Particle Accelerator Conf.* p WEPAF068

[18] Glaesemann G S 2017 Optical fiber mechanical reliability *White Paper* **8002** 1–62

[19] Yang S and Zhang G 2018 A review of interferometry for geometric measurement *Meas. Sci. Technol.* **29** 102001